Supplementary Information for

Oligomeric assembly regulating mitochondrial HtrA2 function as examined by methyl-TROSY NMR

This PDF file includes:

Supplementary text

Figures S1 to S8

SI References

Materials and methods

Protein expression and purification

The human S306A HtrA2 (residues 134-458 Uniprot: O43464) gene was synthesized by GenScript and cloned into a pET-SUMO vector. All HtrA2 mutations were introduced by using Quikchange site-directed mutagenesis (Agilent). For producing non-labeled proteins, transformed *E.coli* BL21(DE3) cells were grown in LB medium at 37 ˚C. Cells were induced by adding 0.2 mM isopropyl β-D-1-thiogalactopyranoside (IPTG) at an OD_{600} of ~0.7 and grown for ~18 hours at 25 ˚C. For producing [U-^{2}H Ileδ1-$^{13}CH_3$, Leuδ1-$^{13}CH_3$, Valγ1-$^{13}CH_3$, Metε-$^{13}CH_3$]- or [U-^{2}H, Ileδ1-$^{13}CH_3$, Leu/Val-$^{13}CH_3/^{12}CD_3$, Metε-$^{13}CH_3$]-labeled proteins (referred to as U-^{2}H, *proR* ILVM-$^{13}CH_3$ or U-^{2}H, ILVM-$^{13}CH_3$ labeling in the text, respectively), the transformed *E.coli* BL21(DE3) cells were grown in minimal M9 D_2O media supplemented with d_7-glucose as the sole carbon source along with the addition

of precursors (60 mg/L 2-keto-3-d_2-4-^{13}C-butyrate for Ileδ1, 80 mg/L 2-keto-3-methyl-d_3-3-d_1-4-^{13}C-butyrate for Leu,Val-$^{13}CH_3/^{12}CD_3$, not stereospecific, 230 mg/L 2-hydroxy-2-methyl-d_3-3-oxobutanoate-4-^{13}C for Leuδ1,Valγ1-$^{13}CH_3$, *proR* stereospecific, and 100 mg/L methyl-$^{13}CH_3$-methionine for Metε) 1 hour before induction of protein overexpression (1, 2). Cells were induced by adding 0.2 mM IPTG at an OD_{600} of ~0.7 and grown for ~18 hours at 25 °C. Proteins were purified by Ni^{2+}-affinity chromatography using a 5 mL HisTrap HP column (GE Healthcare) and eluted in buffer containing 20 mM HEPES-NaOH (pH 7.4), 300 mM NaCl, 300 mM imidazole. The N-terminal His_6-SUMO tag was cleaved by the addition of Ulp1 protease. Protein purification was further achieved by hydrophobic interaction chromatography (HIC) with a Phenyl Superose HR 10/10 column (Pharmacia) using a buffer-gradient of 20 mM HEPES-NaOH (pH 7.4), 0-500 mM $(NH_4)_2SO_4$, 1 mM EDTA, to separate degraded proteins. It should be noted that HtrA2 is susceptible to cleavage by contaminant proteases at the linker connecting the protease and PDZ domains, which could be efficiently suppressed by adding EDTA. The eluted fractions containing full-length proteins were concentrated by using an Amicon Ultra-15 10K MWCO concentrator and subjected to size exclusion chromatography on a Hi-Load 16/600 Superdex 200 pg column (GE Healthcare) in buffer containing 20 mM HEPES-NaOH (pH 7.4), 300 mM NaCl, 1 mM EDTA. The protein concentration was estimated based on absorbance at 280 nm using a molar extinction coefficient of 10,430 M^{-1} cm^{-1}.

The S306A HtrA2 protease domain construct (residues 134-348) was prepared by introducing a stop codon into the S306A HtrA2 (residues 134-458) gene by using Quikchange site-directed mutagenesis. The transformed *E.coli* BL21(DE3) cells grown in minimal M9 D_2O media were supplemented with d_7-glucose as the sole carbon source along with the addition of precursors (60 mg/L 2-keto-3-d_2-4-^{13}C-butyrate for Ileδ1, 80 mg/L 2-keto-3-methyl-d_3-3-d_1-4-^{13}C-butyrate for

Leu,Val-$^{13}CH_3/^{12}CD_3$, and 100 mg/L methyl-$^{13}CH_3$-methionine for Metε) 1 hour before induction. Cells were induced by adding 1.0 mM IPTG at an OD_{600} of ~0.7 and grown for ~18 hours at 25 °C. Proteins were purified by Ni^{2+}-affinity chromatography using a 5 mL HisTrap FF column (GE Healthcare) and eluted in buffer containing 20 mM HEPES-NaOH (pH 7.4), 300 mM NaCl, 300 mM imidazole. The His_6-SUMO tag was cleaved by adding Ulp1 protease, and removed by passage through a 5 mL HisTrap FF column in a buffer of 20 mM HEPES-NaOH (pH 7.4), 300 mM NaCl, 1 mM DTT. The protein solution was concentrated by using an Amicon Ultra-15 10K MWCO concentrator and subjected to size exclusion chromatography on a Superdex 200 Increase 10/300 GL column (GE Healthcare) in buffer containing 20 mM HEPES-NaOH (pH 7.4), 300 mM NaCl, 1 mM EDTA. The protein concentration was estimated based on absorbance at 280 nm using a molar extinction coefficient of 5,960 M^{-1} cm^{-1}.

The gene for the DD-PDZopt peptide (DDGQYYFV), synthesized by using the polymerase chain reaction, was cloned into a pET-SUMO vector with expression as an N-terminal His_6-SUMO-fused peptide. For producing non-labeled peptides, transformed *E.coli* BL21(DE3) cells were grown in LB media at 37 °C. [U-^{2}H]-labeled peptides were generated in the same manner except that transformed *E.coli* BL21(DE3) cells were grown in minimal M9 D_2O media supplemented with d_7-glucose as the sole carbon source. In both cases cells were induced by adding 0.2 mM isopropyl β-D-1-thiogalactopyranoside (IPTG) at an OD_{600} of ~0.7 and grown for ~18 hours at 25 °C. His_6-SUMO-fused peptides were purified by Ni^{2+}-affinity chromatography using a 5 mL HisTrap FF column (GE Healthcare) and eluted in buffer containing 20 mM HEPES-NaOH (pH 7.4), 300 mM NaCl, 300 mM imidazole. The His_6-SUMO-fused peptides were dialyzed into buffer containing 50 mM NH_4HCO_3 (pH 7.0), followed by cleavage of the N-terminal His_6-SUMO tag by the addition of Ulp1 protease. The peptides were separated from the His_6-SUMO tag and Ulp1 by using an Amicon Ultra-15

3K MWCO concentrator and collecting flow-through fractions. The peptides were lyophilized and dissolved into the desired buffer. The peptide concentration was estimated based on the absorbance at 280 nm using a molar extinction coefficient of 2,980 M^{-1} cm^{-1}. In the peptidase assays, synthetic DD-PDZopt peptides (Genscript) were also used after confirming that the synthetic peptides exhibited similar activity to the *E. coli*-expressed version.

NMR experiments

All NMR measurements were performed at 23.5 Tesla (1 GHz ^{1}H frequency) and 40 °C unless indicated otherwise, using a Bruker Ascend spectrometer equipped with a cryogenically cooled *x*, *y*, *z* pulsed-field gradient triple-resonance probe. HtrA2 sample concentrations ranged from 12 – 500 μM in protein (monomer), in an NMR buffer consisting of 20 mM HEPES-NaOH (pD 7.4), 1 mM EDTA, 100% D_2O. ^{13}C-^{1}H HMQC spectra that exploit a methyl-TROSY effect were recorded as described previously (3, 4). All spectra were processed using the *NMRPipe* suite of programs (5) and visualized using the Python package nmrglue (6). Peak intensities were extracted either by using the Peakipy software package (https://github.com/j-brady/peakipy) or by box-sum integration using an in-house Python script.

i) Magnetization exchange

2D ^{13}C[t_1]-t_{mix}-^{1}H[t_2] / 3D ^{13}C[t_1]-t_{mix}-^{13}C[t_2]-^{1}H[t_3] ZZ-exchange experiments were performed using ^{13}C-^{1}H HMQC-based pulse sequences in which an exchange mixing period, t_{mix}, was inserted just after the first ^{13}C frequency labeling period (pulse sequences are available upon request). 2D data were recorded using an 150 μM (monomer) U-^{2}H, *proR* ILVM S306A HtrA2 sample, [NaCl] = 0 mM and 40 °C, with 8 mixing times ranging from 2 to 50 ms, for a net acquisition time of 25.5 hrs. In the 3D

ZZ-exchange experiment, a total of eight 3D-datasets were acquired (~6 days) using mixing times ranging from 2 to 50 ms. For each 3D-dataset, 25% of the total time domain data were non-uniformly-sampled based on a Poisson-Gap sampling schedule (7), and the spectrum was reconstructed using SMILE (8). A 160 μM (monomer) U-^{2}H, *proR* ILVM S306A HtrA2 sample containing 100 μM U-^{2}H DD-PDZopt ([NaCl] = 0 mM) was used.

ii) Rapid timescale dynamics of methyl groups

$S^{2}_{axis}\tau_{c}$ values of side-chain methyl groups were measured by monitoring the build-up of methyl ^{1}H triple quantum coherence as previously described (9), [NaCl] = 0 mM, 50 ˚C. Relaxation delays ranging from 0.5-16 ms or 0.5-18 ms were recorded using 300 μM (monomer) U-^{2}H, *proR* ILVM S306A and 300 μM (monomer) U-^{2}H, *proR* ILVM I441V/S306A (trimer mutant) HtrA2 samples.

iii) Methyl NOEs

A methyl-TROSY based 3D ^{13}C[t_1]-*mix*-^{13}C[t_2]-^{1}H[t_3] NOESY experiment was measured on 300 μM (monomer) U-^{2}H, *proR* ILVM-labeled S306A HtrA2 and 300 μM (monomer) U-^{2}H, *proR* ILVM-labeled S306A/I441V HtrA2 samples with a mixing time of 200 ms, 50 °C, 1 GHz. 75% of the indirect time domain was non-uniformly-sampled using a Poisson-Gap based sampling schedule (7), and the spectrum was reconstructed using SMILE (8).

Methyl group assignments

All of the Ileδ1 (22/22), Leuδ1 (37/37), Metε (5/5), and Valγ1 (37/37) ^{1}H-^{13}C methyl correlations of S306A HtrA2 were assigned by a combined mutagenesis and NOE-based strategy that made use of the crystal structure of HtrA2 (PDB ID: 1LCY) (10). ^{13}C-^{1}H HMQC spectra were recorded of the following assignments mutants in the S306A background: I150L, I164V, I166V, I179V, I193V, I229V, I234V,

I270V, I274V, I295V, I301V, I318V, I329V, I333V, I354V, I362V, I373V, I393V, I397V, I413V, I416V, I441V, L167I, L173I, L192I, L210I, L211I, L266I, L285I, L287I, L369I, L379I, L392I, V135I, V162I, V186I, V199I, V200I, V219I, V220I, V226I, V251I, V257I, V387I, V431I, V439I, V452I, V456I, M260L, M323L, M365I, and M420L. Assignments for peptide-bound HtrA2 were obtained from the analysis of (i) HtrA2 protein dilution experiments in the presence of 1 mM peptide, and (ii) 3D $^{13}C[t_1]$-t_{mix}-$^{13}C[t_2]$-$^{1}H[t_3]$ and $^{1}H[t_1]$-$^{13}C[t_2]$-t_{mix}-$^{1}H[t_3]$ ZZ-exchange magnetization exchange experiments, in which t_{mix} was set to 50 ms.

Fitting of NMR data

Many of the analyses in this manuscript require accurate estimates of populations of various states, such as, for example, trimer and hexamer fractional populations to extract the hexamerization association constant (Fig. 2C & *SI Appendix* Fig. S2D). If relaxation effects can be neglected then peak volumes can be used directly to provide accurate estimates of the required populations. However, because different sized particles are compared (molecular masses of 105 kDa and 210 kDa for trimer and hexamer, respectively), with often different degrees of conformational heterogeneity, it is necessary to take into account the differences in transverse relaxation rates of magnetization that can result. To this end we have adjusted peak volumes to 'correct' for this effect. For example, consider the simple ^{13}C-^{1}H HMQC pulse scheme, where transverse ^{1}H relaxation occurring during a pair of dephasing and rephasing elements, each of duration τ_{CH}, modulates the extracted peak volumes so that they are no longer faithful measures of populations. To mitigate this effect we multiply the extracted values by $exp(R_H 2\tau_{CH})$ where $2\tau_{CH}$ = 7.2 ms and R_H is the apparent ^{1}H transverse relaxation rate, measured as described previously (11).

I) *Trimer-Hexamer equilibrium (Fig. 2C & SI Appendix Fig. S2D)*

We have carried out a series of HtrA2 dilution experiments to measure trimer-hexamer association constants (K_a) in ligand-free and ligand-bound states. Starting from the following thermodynamic scheme,

$$2P_3 \rightleftarrows P_6 \qquad K_a = \frac{[P_6]}{[P_3]^2} \tag{1}$$

and with C_T denoting the total protein concentration (monomer),

$$C_T = 6[P_6] + 3[P_3] \tag{2}$$

we obtain the concentration of the trimer, [P_3], as

$$[P_3] = \frac{-3 + \sqrt{9 + 24K_aC_T}}{12K_a} \tag{3}$$

From which the fractional populations of monomers residing within the trimeric (F_{3mer}) and hexameric (F_{6mer}) states are given by

$$\begin{aligned} F_{3mer} &= \frac{3[P_3]}{C_T} \\ F_{6mer} &= \frac{6[P_6]}{C_T} \end{aligned} \tag{4}$$

In fits for K_a the experimental fractional populations of trimer and hexamer were first obtained by dividing the corrected signal volumes of corresponding cross-peaks derived from trimeric and hexameric states by the sum of the corrected volumes (trimer + hexamer) to get experimental values for F_{3mer} and F_{6mer}. The optimal value of K_a was obtained by computing F_{3mer} and F_{6mer} values according to Eqs. 1-4 and minimizing the residual sum-of-squared (RSS) differences between them and the corresponding experimental values according to

$$RSS = \sum_{j} \sum_{i=1}^{N} \left(F_{j,i}^{exp.}(C_{T,i}) - F_{j,i}^{sim.}(C_{T,i}, K_a) \right)^2 \qquad [5]$$

where $j \in \{3mer, 6mer\}$, $F_{j,i}^{exp.}(C_{T,i})$, and $F_{j,i}^{sim.}(C_{T,i}, K_a)$ are the experimental and fitted data respectively, and the inner sum runs over the total number of experimental data points (*N*) for each species. Minimization of the above target function was achieved using in-house written programs (Python 3.7), exploiting the Nelder-Mead algorithm of the Lmfit python software package (https://lmfit.github.io/lmfit-py/). Distributions of fitted parameters were obtained by running 1,000 Monte-Carlo simulations, and fitted parameter errors were taken as the standard deviations of these parameter sets.

II) *Fit of thermodynamics (Fig. 5B, SI Appendix Figs. S5B, S6&S7B)*

HtrA2 is a homo-oligomeric protein with each protomer containing one DD-PDZopt peptide binding site. Therefore, during the course of a peptide titration experiment a mixture of free, partly-ligated, and fully-ligated states of trimeric and hexameric particles are populated and, in principle, probes from these different states can be observed in NMR spectra, depending on how well resolved the individual signals that derive from them are. A general description of how individual peaks in NMR titration spectra report on the micro-states (and sums thereof) of the system for the case of a homo-oligomeric receptor has been given previously (12). In this section, we describe a number of thermodynamic models that have been used to fit the DD-PDZopt titration profiles to establish that the model of Figure 5C (so called model 3 below) is preferred. We also illustrate the relationship between observed cross-peak intensities and concentrations of the ligated/unligated oligomeric states that are formed during the course of the titration.

a) *Model 1: Hill-type model of ligand binding with infinite positive cooperativity* (*SI Appendix Fig. S6A*)

We assume that the binding of all three ligand molecules (L) to P_3 occurs with infinite cooperativity, and, as described in the main text and illustrated in the scheme of *SI Appendix* Figure S6A, (i) free trimers and hexamers are in equilibrium, bound trimers and hexamers are in equilibrium, and (ii) L does not bind to the hexamer. Under these assumptions the requisite equations are,

$$\begin{aligned} 2P_3 &\rightleftarrows P_6 \qquad K_1 = \frac{[P_6]}{[P_3]^2} \\ P_3 + 3L &\rightleftarrows P_3L_3 \qquad K_2 = \frac{[P_3L_3]}{[P_3][L]^3} \\ 2P_3L_3 &\rightleftarrows P_6L_6 \qquad K_3 = \frac{[P_6L_6]}{[P_3L_3]^2} \end{aligned} \qquad [6]$$

The total protein (monomer) and ligand concentrations are given by

$$\begin{aligned} C_T &= 6[P_6] + 3[P_3] + 3[P_3L_3] + 6[P_6L_6] \\ L_T &= 3[P_3L_3] + 6[P_6L_6] \end{aligned} \qquad [7]$$

where C_T = 150 μM and L_T was varied from 0 to 1 mM during the course of the titration. As discussed in the text we used methyl groups from I362, L377 and M420 as probes of the binding equilibria. Peak volumes in ^{13}C-^{1}H HMQC spectra were obtained, corrected for relaxation effects, expressed in terms of experimental fractional populations by dividing peak volumes by the total volume of all cross-peaks associated with a given methyl probe and relating the resultant value to calculated fractional populations via

Methyl group	Oligomer state	Free/Bound	Fractional population
I362	3mer + 6mer	Free	$(6[P_6] + 3[P_3])/C_T$
	3mer + 6mer	Bound	$(3[P_3L_3] + 6[P_6L_6])/C_T$
L377	6mer	Free	$6[P_6]/C_T$
	3mer	Free	$3[P_3]/C_T$
	3mer + 6mer	Bound	$(3[P_3L_3] + 6[P_6L_6])/C_T$
M420	3mer + 6mer	Free	$(6[P_6] + 3[P_3])/C_T$
	3mer	Bound	$3[P_3L_3]/C_T$
	6mer	Bound	$6[P_6L_6]/C_T$

Recall that peaks observed for each methyl group could be assigned to free 3mer, free 6mer, or bound 3mer, bound 6mer states (depending on the residue; listed under Oligomer State in the above table) based on dilution experiments either in the absence of peptide or under saturating peptide concentrations, and by magnetization exchange experiments which correlate peaks from exchanging states. The interpretation of the free and bound peaks in terms of concentrations of P_3, P_6, P_3L_i and P_6L_i depends, however, on the assignment of the peaks to particular states (listed in the table under "Oligomer state") and on the model that is used to fit the data Thus, for I362 two peaks were observed; one that could be assigned to free protomers and a second to bound protomers (see Figs. 5A & *SI Appendix* Fig. S5A). In this model, where oligomers are either fully bound (*i.e.*, every protomer in the oligomer is ligated) or fully unbound (*i.e.*, every protomer is unligated), the I362 peak intensities can thus be related to

concentrations of states according to I_{free} α 6[P_6]+3[P_3] and I_{bound} α 6[P_6L_6]+3[P_3L_3], as indicated in the table above. In contrast, three peaks are observed for L377, assigned to free hexamers, free trimers or bound trimers+hexamers (*i.e.*, bound protomers for L377 in trimeric and hexameric states are degenerate), so that the concentrations of [P_6] and [P_3] as a function of ligand can be distinguished. For the case of M420 separate peaks are observed reporting on bound protomers in trimers and hexamers, so that [P_6L_6] and [P_3L_3] can be separated, as indicated in the table.

b) *Model 2: step-wise ligand binding to trimer without cooperativity* (*SI Appendix Fig. S6B*)

In this model the peptide ligand is allowed to bind to trimeric HtrA2 in a step-wise manner, with each binding event governed by the same microscopic binding constant (*i.e.*, model of Fig. 5C with $K_2 = K_3 = K_4$), as

$$\begin{aligned}
2P_3 \rightleftarrows P_6 \qquad & K_1 = \frac{[P_6]}{[P_3]^2} \\
P_3 + L \rightleftarrows P_3L \qquad & K_{1st,mac} = \frac{[P_3L]}{[P_3][L]} = 3K_2 \\
P_3L + L \rightleftarrows P_3L_2 \qquad & K_{2nd,mac} = \frac{[P_3L_2]}{[P_3L][L]} = K_2 \\
P_3L_2 + L \rightleftarrows P_3L_3 \qquad & K_{3rd,mac} = \frac{[P_3L_3]}{[P_3L_2][L]} = \frac{1}{3}K_2 \\
2P_3L_3 \rightleftarrows P_6L_6 \qquad & K_3 = \frac{[P_6L_6]}{[P_3L_3]^2}
\end{aligned} \qquad [8]$$

Note that $K_{x,mac}$(K_2) is a macroscopic(microscopic) binding constant. The factors 3 and 1/3 take into account the three ways in which L can bind to P_3 to form P_3L or in which L can be removed from P_3L_3 to generate P_3L_2. With mass conservation,

$$\begin{aligned}
C_T &= 6[P_6] + 3[P_3] + 3[P_3L] + 3[P_3L_2] + 3[P_3L_3] + 6[P_6L_6] \\
L_T &= [P_3L] + 2[P_3L_2] + 3[P_3L_3] + 6[P_6L_6]
\end{aligned} \qquad [9]$$

it follows that the relations between the observed oligomeric states and the fractional populations measured by NMR are

Methyl group	Oligomer state	Free/Bound	Fractional population
I362	3mer + 6mer	Free	$(6[P_6] + 3[P_3] + 2[P_3L] + [P_3L_2])/C_T$
	3mer + 6mer	Bound	$([P_3L] + 2[P_3L_2] + 3[P_3L_3] + 6[P_6L_6])/C_T$
L377	6mer	Free	$6[P_6]/C_T$
	3mer	Free	$(3[P_3] + 2[P_3L] + [P_3L_2])/C_T$
	3mer + 6mer	Bound	$([P_3L] + 2[P_3L_2] + 3[P_3L_3] + 6[P_6L_6])/C_T$
M420	3mer + 6mer	Free	$(6[P_6] + 3[P_3] + 2[P_3L] + [P_3L_2])/C_T$
	3mer	Bound	$([P_3L] + 2[P_3L_2] + 3[P_3L_3])/C_T$
	6mer	Bound	$6[P_6L_6]/C_T$

The distinguishing feature between Models 1 and 2 is that in Model 2 populations of partially bound oligomer can be present, in addition to fully bound or unbound particles. Thus, in the case of I362 the free 6mer+3mer peak, for example, originates from all oligomeric states with one or more unligated protomers, with the prefactors in the listed "Fractional population column" in the table taking into account the number of unligated protomers in each particle from which signal derives (3-*i* unligated protomers in $[P_3L_i]$).

c) *Model 3: step-wise ligand binding to trimer with cooperativity* (*Fig. 5*)

In model 3 (Fig. 5C) L is allowed to bind to the trimeric state of HtrA2 in a step-wise manner with different microscopic binding constants for each step, as

$$\begin{aligned} 2P_3 &\rightleftarrows P_6 & K_1 &= \frac{[P_6]}{[P_3]^2} \\ P_3 + L &\rightleftarrows P_3L & K_{mac,2} &= \frac{[P_3L]}{[P_3][L]} = 3K_2 \\ P_3L + L &\rightleftarrows P_3L_2 & K_{mac,3} &= \frac{[P_3L_2]}{[P_3L][L]} = K_3 \\ P_3L_2 + L &\rightleftarrows P_3L_3 & K_{mac,4} &= \frac{[P_3L_3]}{[P_3L_2][L]} = \frac{1}{3}K_4 \\ 2P_3L_3 &\rightleftarrows P_6L_6 & K_5 &= \frac{[P_6L_6]}{[P_3L_3]^2} \end{aligned} \qquad [10]$$

and the mass conservation terms and NMR fractional populations are defined as in model 2.

As described in the text, we have done measurements with [NaCl] = 0 mM (Fig. 5) and 120 mM (*SI Appendix* Fig. S5). Similar changes in the populations of each the states were observed using the I362, L377, and M420 methyl probes in both cases, confirming the preferential ligand binding to the trimer (*SI Appendix* Figs. 5C&S5C). As the hexamerization affinity in both the free and bound states was markedly stronger at the high salt concentration (5.6-fold and 23-fold in the free and bound state, respectively), the populations of the free and fully bound trimer states were much lower than in the absence of salt, complicating the fits when [NaCl] = 120 mM. To constrain the fits in this case (high salt) we focused only on probes from I362 and M420; the free 3mer peak for L377 was very broad and could not be properly quantified. For I362 and M420 only the free and bound peaks were well-resolved, so that the information content of the spectra was more limited in the studies at 120 mM salt. Values of the trimer-hexamer association constants for the ligand free- and fully bound-states (K_1 and K_5, above) were fixed to the values obtained from the HtrA2 dilution experiments (K_1 = 2.9 $\times 10^5$ M^{-1} and K_5 = 6.9 $\times 10^4$

M^{-1}), and the successive ligand-binding constants, K_2, K_3, and K_4, were constrained to follow the relation $K_3/K_2 = K_4/K_3$, in order to restrict the parameter space. Note that in our unconstrained fits of the titration for [NaCl] = 0 mM we obtained $K_3/K_2 \sim K_4/K_3$, which provided the motivation for using these constraints for the high salt data. With these assumptions, the three DD-PDZopt association constants, K_2, K_3, and K_4 were calculated to be 1.0 ± 0.1 $\times 10^4$ M^{-1}, 1.43 ± 0.04 $\times 10^4$ M^{-1}, and 2.1 ± 0.2 $\times 10^4$ M^{-1}, with $K_3/K_2 = K_4/K_3 = 1.4 \pm 0.2$ (high salt). The relation between the corrected volumes of methyl peaks derived from I362 and M420 and the concentrations of the various ligated states for the high salt case are given below (and for the low salt case where peak resolution was better so that separate bound peaks were observed for M420 3mer and 6mer the relations are listed above as for Model 2):

Methyl group	Oligomer state	Free/Bound	Fractional population
I362	3mer + 6mer	Free	$(6[P_6] + 3[P_3] + 2[P_3L] + [P_3L_2])/C_T$
	3mer + 6mer	Bound	$([P_3L] + 2[P_3L_2] + 3[P_3L_3] + 6[P_6L_6])/C_T$
M420	3mer + 6mer	Free	$(6[P_6] + 3[P_3] + 2[P_3L] + [P_3L_2])/C_T$
	3mer + 6mer	Bound	$([P_3L] + 2[P_3L_2] + 3[P_3L_3] + 6[P_6L_6])/C_T$

d) Model 4: step-wise ligand binding to trimer and hexamer with cooperativity (*SI Appendix Fig. S7*)

In the model we expand scheme 3 (Fig. 5C & *SI Appendix* Fig. S6C) to add ligand binding to P_6 and P_6L (*SI Appendix* Fig. S7). Our goal in using this model was to assess the importance of ligand binding to the hexameric form of HtrA2 in a quantitative manner; recall that from the profile of the bound 6mer peak (M420; Fig. 5B) it is clear that the population of bound hexamer lags far behind the bound trimer, with

no bound 6mer for the first half of the titration. In this case we can write,

$$\begin{aligned}
2P_3 \rightleftarrows P_6 \qquad & K_1 = \frac{[P_6]}{[P_3]^2} \\
P_3 + L \rightleftarrows P_3L \qquad & K_{mac,2} = \frac{[P_3L]}{[P_3][L]} = 3K_2 \\
P_3L + L \rightleftarrows P_3L_2 \qquad & K_{mac,3} = \frac{[P_3L_2]}{[P_3L][L]} = K_3 \\
P_3L_2 + L \rightleftarrows P_3L_3 \qquad & K_{mac,4} = \frac{[P_3L_3]}{[P_3L_2][L]} = \frac{1}{3}K_4 \\
2P_3L_3 \rightleftarrows P_6L_6 \qquad & K_5 = \frac{[P_6L_6]}{[P_3L_3]^2} \\
P_6 + L \rightleftarrows P_6L \qquad & K_{mac,6} = \frac{[P_6L]}{[P_6][L]} = 6K_6 \\
P_6L + L \rightleftarrows P_6L_2 \qquad & K_{mac,7} = \frac{[P_6L_2]}{[P_6L][L]} = \frac{5}{2}K_7
\end{aligned} \tag{11}$$

and

$$\begin{aligned}
C_T &= 6[P_6] + 6[P_6L] + 6[P_6L_2] + 6[P_6L_6] + 3[P_3] + 3[P_3L] + 3[P_3L_2] + 3[P_3L_3] \\
L_T &= [P_3L] + 2[P_3L_2] + 3[P_3L_3] + [P_6L] + 2[P_6L_2] + 6[P_6L_6]
\end{aligned} \tag{12}$$

with the relationship between the free/bound peaks for the various oligomeric states and the concentrations of the individual microstates given by,

Methyl group	Oligomer state	Free/Bound	Fractional population
I362	3mer + 6mer	Free	$(6[P_6] + 5[P_6L] + 4[P_6L_2] + 3[P_3] + 2[P_3L] + [P_3L_2])/C_T$
	3mer + 6mer	Bound	$([P_3L] + 2[P_3L_2] + 3[P_3L_3] + [P_6L] + 2[P_6L_2] + 6[P_6L_6])/C_T$
L377	6mer	Free	$(6[P_6] + 5[P_6L] + 4[P_6L_2])/C_T$
	3mer	Free	$(3[P_3] + 2[P_3L] + [P_3L_2])/C_T$
	3mer + 6mer	Bound	$([P_3L] + 2[P_3L_2] + 3[P_3L_3] + [P_6L] + 2[P_6L_2] + 6[P_6L_6])/C_T$
M420	3mer + 6mer	Free	$(6[P_6] + 5[P_6L] + 4[P_6L_2] + 3[P_3] + 2[P_3L] + [P_3L_2])/C_T$
	3mer	Bound	$([P_3L] + 2[P_3L_2] + 3[P_3L_3])/C_T$
	6mer	Bound	$([P_6L] + 2[P_6L_2] + 6[P_6L_6])/C_T$

Only the higher quality profiles recorded at 0 mM NaCl were analyzed using this model.

As described above, in all fits of titration profiles to thermodynamic models the NMR experimentally derived peak intensities are initially normalized to obtain experimental fractional populations, $F^{exp.}$, by dividing the corrected volume of a given peak by the sum of corrected volumes of all peaks associated with that methyl probe. The optimal association constants for a given model were obtained using a nested minimization routine in which the experimental fractional populations were compared to the simulated fractional populations, $F^{sim.}$, using expressions for fractional populations listed in the tables above. Briefly, this was accomplished according to the following scheme which involves a pair of minimization steps. In the first minimization the experimentally determined C_T and L_T values along with initial association constant estimates were passed into Python 3.7's SciPy 1.3 library

root-finding algorithm *scipy.optimize.root* to determine the free and ligand-bound protein concentrations. This is achieved by solving systems of equations relating protein concentrations to equilibrium constants and C_T and L_T values, as per Eqs 6-12. In the second minimization step the extracted concentrations were used to compute fractional populations for free and bound trimer and hexamer states to compare with the experimental data via

$$RSS = \sum_{k} \sum_{j} \sum_{i=1}^{N} \left(F_{k,j,i}^{exp.}(C_T, L_{T,i}) - F_{k,j,i}^{sim.}(C_T, L_{T,i}, \zeta) \right)^2 \qquad [13]$$

where $k \in \{free, bound\}$, $j \in \{3mer, 6mer\}$, N is the total number of titration points fitted, $L_{T,i}$ is the i^{th} total ligand concentration in the titration, and ζ is the set of association constants to be optimized for a given model. The association constants were then incremented and the minimization returned to the first step to calculate 'better' estimates of concentrations. Once the minimum RSS value was reached, the optimal parameters for the employed model were returned. Minimization of the above target function was achieved using in-house written programs (Python 3.7), exploiting the Nelder-Mead algorithm of the Lmfit python software package (https://lmfit.github.io/lmfit-py/). Distributions of fitted parameters were obtained by running 1,000 Monte-Carlo simulations, and fitted parameter errors were taken as the standard deviations of these parameter sets.

III) *Fits of magnetization exchange* (Figs. 2D)

The dimer-hexamer exchange data were fit to equations described previously (13–15) to extract rate constants. The kinetic model includes two different magnetization terms corresponding to hexameric and trimeric states, M_{P_6} and M_{P_3}. The flow of the magnetization during the mixing period was calculated using the following matrix differential equation,

$$\frac{d}{dt}\vec{M} = (\vec{K} - \vec{R})\vec{M}$$
$$\vec{M} = \begin{bmatrix} M_{P_6} \\ M_{P_3} \end{bmatrix} \qquad [14]$$

The kinetic ($\vec{K}$) and relaxation ($\vec{R}$) matrices were defined as follows,

$$\vec{K} = \begin{bmatrix} -k_{off} & 2k_{on}[P_3] \\ k_{off} & -2k_{on}[P_3] \end{bmatrix}$$
$$\vec{R} = \begin{bmatrix} R_{P_6} & 0 \\ 0 & R_{P_3} \end{bmatrix} \qquad [15]$$

where k_{on} and k_{off} are the on- (3mer to 6mer) and off- (6mer to 3mer) rates for the trimer-hexamer equilibrium, and R_{P_6} and R_{P_3} are the effective relaxation rates during the mixing period. The solution to Eq. [15] is given by

$$\begin{aligned} I_{P_6}^{calc.}(t) &= c\begin{bmatrix} 1 & 0 \end{bmatrix} exp\{(\vec{K} - \vec{R})t)\} \begin{bmatrix} M_{P_6} \\ 0 \end{bmatrix} \\ I_{P_3}^{calc.}(t) &= c\begin{bmatrix} 0 & 1 \end{bmatrix} exp\{(\vec{K} - \vec{R})t)\} \begin{bmatrix} 0 \\ M_{P_3} \end{bmatrix} \\ I_{P_6 \rightleftarrows P_3}^{calc.}(t) &= c\begin{bmatrix} 0 & 1 \end{bmatrix} exp\{(\vec{K} - \vec{R})t)\} \begin{bmatrix} M_{P_6} \\ 0 \end{bmatrix} \\ &= c\begin{bmatrix} 1 & 0 \end{bmatrix} exp\{(\vec{K} - \vec{R})t)\} \begin{bmatrix} 0 \\ M_{P_3} \end{bmatrix} \end{aligned} \qquad [16]$$

where $I_{P_6}^{calc.}(t)$ and $I_{P_3}^{calc.}(t)$ are the volumes of the diagonal peaks from hexamer and ($I_{P_3}^{calc.}(t)$) trimer, respectively, $I_{P_6 \rightleftarrows P_3}^{calc.}(t)$ is the volume of the exchange cross-peaks, and c is a constant of proportionality that converts magnetization to peak volume. Values of [P_6] and [P_3] can be obtained from Eqs 1-3 using k_{on} and k_{off} values that are generated during the fits of the exchange data ($K_a = k_{on}/k_{off}$) and at thermal equilibrium each magnetization component can be calculated in terms of the concentrations of hexameric and trimeric species as follows,

$$M_{P_6} \propto 6[P_6]$$
$$M_{P_3} \propto 3[P_3] \qquad [17]$$

We have used the time evolution of peaks from V452 to extract k_{on} and k_{off}, after first taking into account the effects of transverse relaxation during the course of the magnetization exchange pulse scheme. In the fits of the data the average of the two exchange cross-peaks ($I^{exp.}_{P_6 \rightleftarrows P_3}$), were used.

Optimized exchange rate constants and relaxation rates were obtained in a minimization routine by comparing the experimentally observed peak volumes to the simulated ZZ-exchange profiles. Briefly, this was accomplished as follows. In step 1, $K_a = k_{on}/k_{off}$ was calculated from initial values of the rate constants and used along with C_T to obtain the hexamer and trimer concentrations, [P_6] and [P_3], via Eqs. 1-3. In step 2, these concentrations were converted to initial magnetization values (t=0, Eq. 17) and, along with the kinetic rate constants, subsequently used to simulate ZZ-exchange time profiles for comparison with the experimental data,

$$RSS = \sum_j \sum_{i=1}^{N} \left(I_j^{exp.}(C_T, t_i) - I_j^{calc.}(C_T, t_i, \zeta)\right)^2 \qquad [18]$$
$$j \in \{P_6, P_3, P_6 \rightleftarrows P_3\}$$

where N is the total number of time points, t_i is the i^{th} mixing period, and ζ is the set of parameters to be optimized $(c, k_{on}, k_{off}, R_{P_6}, R_{P_3})$. The extracted parameters were then used to recalculate concentrations and step 2 repeated in an iterative manner until a minimum in RSS was achieved. Minimization of the above target function made use of in-house written programs (Python 3.7), exploiting the Nelder-Mead algorithm of the Lmfit python software package (https://lmfit.github.io/lmfit-py/). Distributions of fitted parameters were obtained by running 1,000 Monte-Carlo simulations, and fitted parameter errors were taken as the standard deviations of these parameter sets.

Analysis of the kinetics data describing hexamerization and ligand binding (Fig. 6) is more complex since a mixture of free, partly-ligated, and fully-ligated states of trimeric and hexameric particles are populated and a given molecular species, such as P_3L_i, can contribute to intensities of peaks derived from unbound and bound protomers (*i.e.*, P_3L_i contains 3-i unbound and i bound protomers). Thus, a given free or bound peak can contain information regarding populations of several differentially-ligated states (as is clear in expressions for populations for the thermodynamic models considered above) that must be properly sorted to extract meaningful kinetics data. A general description of how this is accomplished in the context of a homo-oligomeric receptor, as well as the kinetic equations describing the evolution of magnetization in such a system, have been given previously (12). In what follows we include contributions from trimer-hexamer exchange previously omitted. In order to simplify the expressions, we assume that DD-PDZopt exclusively binds to protomers in the trimeric state with the same ligand association constants and ligand off/on rates for each successive binding event (effectively model 2 above) so as to minimize the number of fitting parameters. As the population of P_6L_6 is negligibly small (< 0.1 %) under our experimental conditions (C_T = 160 μM, L_T = 100 μM, 40 ˚C, 0 mM NaCl) we did not include P_6L_6 state in the model (Fig. 6). The kinetic model includes seven different magnetization terms, $M_{p,q}$ $(p \in \{U, B\}\ q \in \{P_6, P_3, P_3L, P_3L_2, P_3L_3\})$, where U and B denote unbound and bound protomers, respectively,

$$\vec{M} = [\, M_{U,P_6} \quad M_{U,P_3} \quad M_{U,P_3L} \quad M_{U,P_3L_2} \quad M_{B,P_3L} \quad M_{B,P_3L_2} \quad M_{B,P_3L_3} \,]^{+} \qquad [19]$$

where + denotes the transpose operator. For example, M_{U,P_3L} and M_{B,P_3L} are the magnetization components arising from unbound and bound protomers in the P_3L chemical species, respectively. In thermal equilibrium, each magnetization component listed above can be calculated in terms of the

concentrations of the different states as follows,

$$\begin{aligned} M_{U,P_6} &\propto 6[P_6] \\ M_{U,P_3} &\propto 3[P_3] \\ M_{U,P_3L} &\propto 2[P_3L] \\ M_{U,P_3L_2} &\propto [P_3L_2] \\ M_{B,P_3L} &\propto [P_3L] \\ M_{B,P_3L_2} &\propto 2[P_3L_2] \\ M_{B,P_3L_3} &\propto 3[P_3L_3] \end{aligned} \qquad [20]$$

Following a lengthy derivation given previously (12), a kinetic matrix, $\vec{K}$, is obtained, where $k_{1,\text{on}}$ and $k_{1,\text{off}}$ are the on- and off-rates for the trimer-hexamer equilibrium, and $k_{2,\text{on}}$ and $k_{2,\text{off}}$ are the microscopic on- and off-rates for DD-PDZopt binding (Fig. 6). The effects of relaxation, in this case of ^{1}H-^{13}C two-spin order, can be added in an ad-hoc manner via the $\vec{R}$ matrix,

$$\vec{K} = \begin{bmatrix} -k_{1,off} & 2k_{1,on}[P_3] & 0 & 0 & 0 & 0 & 0 \\ k_{1,off} & -2k_{1,on}[P_3] - 3k_{2,on}[L] & k_{2,off} & 0 & k_{2,off} & 0 & 0 \\ 0 & 2k_{2,on}[L] & -k_{2,off} - 2k_{2,on}[L] & 2k_{2,off} & 0 & k_{2,off} & 0 \\ 0 & 0 & k_{2,on}[L] & -2k_{2,off} - k_{2,on}[L] & 0 & 0 & k_{2,off} \\ 0 & k_{2,on}[L] & 0 & 0 & -k_{2,off} - 2k_{2,on}[L] & k_{2,off} & 0 \\ 0 & 0 & k_{2,on}[L] & 0 & 2k_{2,on}[L] & -2k_{2,off} - k_{2,on}[L] & 2k_{2,off} \\ 0 & 0 & 0 & k_{2,on}[L] & 0 & k_{2,on}[L] & -3k_{2,off} \end{bmatrix} \qquad [21]$$

$$\vec{R} = \begin{bmatrix} R_{U,P_6} & 0 & 0 & 0 & 0 & 0 & \\ 0 & R_{U,P_3} & 0 & 0 & 0 & 0 & 0 \\ 0 & 0 & R_{U,P_3L} & 0 & 0 & 0 & 0 \\ 0 & 0 & 0 & R_{U,P_3L_2} & 0 & 0 & 0 \\ 0 & 0 & 0 & 0 & R_{B,P_3L} & 0 & 0 \\ 0 & 0 & 0 & 0 & 0 & R_{B,P_3L_2} & 0 \\ 0 & 0 & 0 & 0 & 0 & 0 & R_{B,P_3L_3} \end{bmatrix} \qquad [22]$$

The time-evolution of magnetization is calculated by solving

$$\frac{d}{dt}\vec{M} = (\vec{K} - \vec{R})\vec{M} \qquad [23]$$

where values of the magnetization components at t=0 were calculated using Eq. 20. The concentrations of each chemical species at the given total HtrA2 monomer and DD-PDZopt concentrations were

calculated using the relationships, $K_1 = k_{1,on}/k_{1,off}$, $K_2 = k_{2,on}/k_{2,off}$, and Eqs. 8-9.

As described in the text, we have used the time evolution of cross-peaks from V452 to extract the required rate constants. V452 gave rise to three resolved peaks (corrected volumes denoted by I in what follows) corresponding to unbound protomers in hexamers (I_{U,P_6}), unbound protomers in trimers ($I_{U,(P_3+P_3L+P_3L_2)}$), and bound protomers in trimers ($I_{B,(P_3L+P_3L_2+P_3L_3)}$). Note that the unbound trimer and hexamer peaks and the bound trimer peaks contain contributions from magnetization terms as follows:

$$\begin{aligned} I_{U,P_6} &\propto M_{U,P_6} \\ I_{U,(P_3+P_3L+P_3L_2)} &\propto M_{U,P_3} + M_{U,P_3L} + M_{U,P_3L_2} \\ I_{B,(P_3L+P_3L_2+P_3L_3)} &\propto M_{B,P_3L} + M_{B,P_3L_2} + M_{B,P_3L_3} \end{aligned} \qquad [24]$$

The volumes of diagonal- and cross-peaks in the magnetization exchange experiment can be calculated according to

$$\begin{aligned} I^{calc.}_{U,P_6}(t) &= c\,[\,1 \quad 0 \quad 0 \quad 0 \quad 0 \quad 0 \quad 0\,]\, exp\{(\vec{K}-\vec{R})t)\} \\ &\quad \times [\,M_{U,P_6} \quad 0 \quad 0 \quad 0 \quad 0 \quad 0 \quad 0\,]^{+} \\ I^{calc.}_{U,(P_3+P_3L+P_3L_2)}(t) &= c\,[\,0 \quad 1 \quad 1 \quad 1 \quad 0 \quad 0 \quad 0\,]\, exp\{(\vec{K}-\vec{R})t)\} \\ &\quad \times [\,0 \quad M_{U,P_3} \quad M_{U,P_3L} \quad M_{U,P_3L_2} \quad 0 \quad 0 \quad 0\,]^{+} \\ I^{calc.}_{B,(P_3L+P_3L_2+P_3L_3)}(t) &= c\,[\,0 \quad 0 \quad 0 \quad 0 \quad 1 \quad 1 \quad 1\,]\, exp\{(\vec{K}-\vec{R})t)\} \\ &\quad \times [\,0 \quad 0 \quad 0 \quad 0 \quad M_{B,P_3L} \quad M_{B,P_3L_2} \quad M_{B,P_3L_3}\,]^{+} \end{aligned} \qquad [25]$$

for the diagonal peaks, and, for the cross-peaks

$$
\begin{aligned}
I^{calc.}_{U,6mer\rightleftarrows U,3mer}(t) &= c\begin{bmatrix}0 & 1 & 1 & 1 & 0 & 0 & 0\end{bmatrix} exp\{(\vec{K}-\vec{R})t)\} \\
&\quad \times \begin{bmatrix}M_{U,P_6} & 0 & 0 & 0 & 0 & 0 & 0\end{bmatrix}^{+} \\
&= c\begin{bmatrix}1 & 0 & 0 & 0 & 0 & 0 & 0\end{bmatrix} exp\{(\vec{K}-\vec{R})t)\} \\
&\quad \times \begin{bmatrix}0 & M_{U,P_3} & M_{U,P_3L} & M_{U,P_3L_2} & 0 & 0 & 0\end{bmatrix}^{+} \\
I^{calc.}_{U,3mer\rightleftarrows B,3mer}(t) &= c\begin{bmatrix}0 & 0 & 0 & 0 & 1 & 1 & 1\end{bmatrix} exp\{(\vec{K}-\vec{R})t)\} \\
&\quad \times \begin{bmatrix}0 & M_{U,P_3} & M_{U,P_3L} & M_{U,P_3L_2} & 0 & 0 & 0\end{bmatrix}^{+} \\
&= c\begin{bmatrix}0 & 1 & 1 & 1 & 0 & 0 & 0\end{bmatrix} exp\{(\vec{K}-\vec{R})t)\} \\
&\quad \times \begin{bmatrix}0 & 0 & 0 & 0 & M_{B,P_3L} & M_{B,P_3L_2} & M_{B,P_3L_3}\end{bmatrix}^{+} \\
I^{calc.}_{U,6mer\rightleftarrows B,3mer}(t) &= c\begin{bmatrix}1 & 0 & 0 & 0 & 0 & 0 & 0\end{bmatrix} exp\{(\vec{K}-\vec{R})t)\} \\
&\quad \times \begin{bmatrix}0 & 0 & 0 & 0 & M_{B,P_3L} & M_{B,P_3L_2} & M_{B,P_3L_3}\end{bmatrix}^{+} \\
&= c\begin{bmatrix}0 & 0 & 0 & 0 & 1 & 1 & 1\end{bmatrix} exp\{(\vec{K}-\vec{R})t)\} \\
&\quad \times \begin{bmatrix}M_{U,P_6} & 0 & 0 & 0 & 0 & 0 & 0\end{bmatrix}^{+}
\end{aligned}
\qquad [26]
$$

where it is understood that,

$$
\begin{aligned}
I_{U,6mer\rightleftarrows U,3mer} &= I_{U,P_6\rightleftarrows U,(P_3+P_3L+P_3L_2)} \\
I_{U,3mer\rightleftarrows B,3mer} &= I_{U,(P_3+P_3L+P_3L_2)\rightleftarrows B,(P_3L+P_3L_2+P_3L_3)} \\
I_{U,6mer\rightleftarrows B,3mer} &= I_{U,P_6\rightleftarrows B,(P_3L+P_3L_2+P_3L_3)}
\end{aligned}
\qquad [27]
$$

so that the three terms in Eq. 26 quantify magnetization exchange between unbound protomers in exchanging hexamers and trimers ($I^{calc.}_{U,6mer\rightleftarrows U,3mer}(t)$), between unbound and bound protomers in trimers ($I^{calc.}_{U,3mer\rightleftarrows B,3mer}(t)$), and between unbound protomers in a hexamer and bound protomers in a trimer ($I^{calc.}_{U,6mer\rightleftarrows B,3mer}(t)$). In Eqs. 25-26 c denotes a constant of proportionality that converts magnetization to signal volume. In the analysis of the data we have assumed three fitted relaxation rates, R_{U,P_6}, $R_{U,P_3} = R_{U,P_3L} = R_{U,P_3L_2}$, and $R_B = R_{B,P_3L} = R_{B,P_3L_2} = R_{B,P_3L_3}$ and have averaged volumes of exchange cross-peaks prior to analysis.

Optimization was carried out by comparing experimentally observed and computed peak

volumes using the same procedure as described for optimization of the hexamer ⇄ trimer kinetic rates above. Briefly, values for C_T, L_T, and initial estimates for the rate constants were used to obtain initial guesses for $K_1 = k_{1,on}/k_{1,off}$ and $K_2 = k_{2,on}/k_{2,off}$, from which a set of protein concentrations, P_3L_i, P_6L_i were calculated. These concentrations were converted to initial magnetization values via Eq. 20 and then used to simulate ZZ-exchange time profiles for comparison with the experimental data,

$$RSS = \sum_j \sum_{i=1}^{N} \left(I_j^{exp.}(C_T, L_T, t_i) - I_j^{calc.}(C_T, L_T, t_i, \zeta)\right)^2 \quad [28]$$

$$j \in \{(U, P_6), (U, (P_3 + P_3L + P_3L_2)), (B, (P_3L + P_3L_2 + P_3L_3)), \\ (U, 6mer \rightleftarrows U, 3mer), (U, 3mer \rightleftarrows B, 3mer), (U, 6mer \rightleftarrows B, 3mer)\}$$

where N is the total number of time points, t_i is the i^{th} mixing period, and ζ is the set of parameters to be optimized $(c, k_{1,on}, k_{1,off}, k_{2,on}, k_{2,off}, R_{U,P_6}, R_{U,P_3}, R_B)$. This process was reiterated until a minimum RSS value was obtained, exploiting the Nelder-Mead algorithm of the Lmfit python software package (https://lmfit.github.io/lmfit-py/). Distributions of fitted parameters were obtained by running 1,000 Monte-Carlo simulations, and fitted parameter errors were taken as the standard deviations of these parameter sets.

IV) *Extraction of fast-timescale dynamics parameters*

$S^2_{axis}\tau_c$ values of side-chain methyl groups were obtained by fitting the ratios of cross-peaks extracted from spectra quantifying sums (I_{SQ}) and differences (I_{3Q}) of single quantum methyl ^{1}H magnetization components as a function of a delay (T) during which transverse single quantum magnetization evolves,

$$\left|\frac{I_{3Q}}{I_{SQ}}\right| = \frac{0.75\,\eta\,tanh(T\sqrt{\eta^2+\delta^2})}{\sqrt{\eta^2+\delta^2} - \delta\,tanh(T\sqrt{\eta^2+\delta^2})} \quad [29]$$

In Eq. 29 the intra-methyl ^{1}H–^{1}H dipolar cross-correlated relaxation rate, η, is given by

$$\eta \approx \frac{9}{10}\left(\frac{\mu_0}{4\pi}\right)^2 [P_2(cos\theta_{axis,HH})]^2 \frac{S^2_{axis}\gamma_H^4 \hbar^2 \tau_c}{r_{HH}^6} \qquad [30]$$

where γ_H is the gyromagnetic ratio of a ^{1}H spin, r_{HH} is the distance between methyl protons (1.813Å), $P_2(x) = \frac{1}{2}(3cos^2 x - 1)$, $\hbar$ is Planck's constant divided by 2π, and $\theta_{axis,HH}$ (90°) is the angle between a vector connecting pairs of methyl protons and the methyl 3-fold symmetry axis. The fitted η, and δ were extracted by minimizing the following target function.

$$RSS = \sum_i^N \left(\left| \frac{I_{3Q}^{exp.}(T_i)}{I_{SQ}^{exp.}(T_i)} \right| - \left| \frac{I_{3Q}}{I_{SQ}} \right|_{T_i,\eta,\delta}^{calc.} \right)^2 \qquad [31]$$

where $I_{3Q}^{exp.}(T)$ and $I_{SQ}^{exp.}(T)$ are the volumes of the experimentally observed cross-peaks at *T,* and $\left| \frac{I_{3Q}}{I_{SQ}} \right|_{T_i,\eta,\delta}^{calc.}$ is the simulated ratio at given *T*, η, and δ obtained using Eq. 29. Minimization of the above target function was achieved using in-house written programs (Python 3.7), exploiting the Nelder-Mead algorithm of the Lmfit python software package (https://lmfit.github.io/lmfit-py/). The standard deviations of the fitted parameters were estimated using the covariance matrix method (16).

SAXS experiments

SAXS measurements for molecular weight calculations were performed using the Anton-Paar SAXSpace platform. Measurements were performed in buffer containing 20 mM HEPES-NaOH (pH 7.4), 0 or 120 mM NaCl, 1 mM EDTA, and 2% glycerol, and with a protein concentration of 5 mg/mL (143 μM in monomer). Datasets were collected at 40 °C for 2 hrs, and a buffer blank was subtracted for

each dataset. Data were analyzed using the ATSAS 3.0.2 suite of programs (17). The molecular weight calculations used the Bayesian inference approach (18), implemented in the software package *PRIMUS* (19). SAXS profiles for structural modeling of the HtrA2 hexamer were obtained at the SIBYLS beamline of the Advanced Light Source at Lawrence Berkeley National Laboratory (20). Measurements of S306A HtrA2 were performed in a buffer containing 20 mM HEPES-NaOH (pH 7.4), 120 mM NaCl, 1 mM EDTA, and 2% glycerol, with four different protein concentrations (1, 2, 5, and 10 mg/mL). Datasets were collected at 23-26 ^{o}C with 0.3 sec exposures for 10 sec, and a buffer blank was subtracted from each exposure. Each buffer-subtracted exposure was checked for radiation damage and the exposures without significant radiation damage were merged to produce a final curve using the SAXS FrameSlice online server (https://sibyls.als.lbl.gov/ran/). The radii of gyration (R_g) were obtained using the *AUTORG* module implemented in *PRIMUS*. Rigid-body docking was performed using the *SASREFMX* program (21). A starting HtrA2 structure (trimer) was used, generated by filling in the disordered loops using the *SWISS-MODEL* server (22), with the available crystal structure of the HtrA2 trimer as a template (PDB ID: 1LCY). In the docking calculation a distance restraint of 7Å between the Y451 Cα atom of one trimer and any Cα atom of a second trimer was used; otherwise standard settings were employed. Experimental SAXS profiles and the structural model of the hexamer have been deposited in the Small Angle Scattering Biological Data Bank (accession codes: SASDKL4, SASDKM4, SASDKN4, and SASDKP4).

Peptidase assay

The peptidase activity of HtrA2 was measured at 40 ^{o}C using the peptide

Mca-IRRVSYSF{Lys(Dnp)}KK (Dnp: N-dinitrophenyldiaminopropionic acid) (GenScript) as substrate, in which a fluorogenic 7-methoxy-coumarin-4-acetic acid (Mca) group was attached to the N-terminus (23). The reaction was monitored with a Synergy Neo2 96-well microplate reader every 21 seconds using λ_{ex}: 320 nm, λ_{em}: 390 nm with 10 nm bandwidths. Measurements were conducted with 200 nM (for 0 mM NaCl) or 500 nM (for 120 mM NaCl) U-^{2}H HtrA2 (wild-type) and 22 μM substrate peptide, unless otherwise indicated, dissolved in buffer containing 20 mM HEPES-NaOH (pD 7.4), 0 or 120 mM NaCl, and 1 mM EDTA in D_2O. The measured fluorescence intensity was converted to concentration of the cleaved product by using the fluorescence of the N-terminally Mca-modified IRRV peptide (Genscript) as a standard. Catalytic rates are derived from initial rates extracted and analyzed using an in-house Python script. Error bars correspond to one standard deviation based on three repeat measurements. The cleavage rate of Mca-IRRVSYSF{Lys(Dnp)}KK as a function of DD-PDZopt concentration was fit to the standard one-site binding model assuming the total peptide concentration can be well approximated by the free peptide concentration, $k = k_{max}[\text{DD-PDZopt}]/(K_{D,app}+[\text{DD-PDZopt}]) + k_0$, where k is the substrate cleavage rate, k_0 is the basal substrate cleavage rate in the absence of DD-PDZopt, k_{max} is the maximum cleavage rate in the fully peptide-bound form, $K_{D,app}$ is the apparent microscopic dissociation constant.

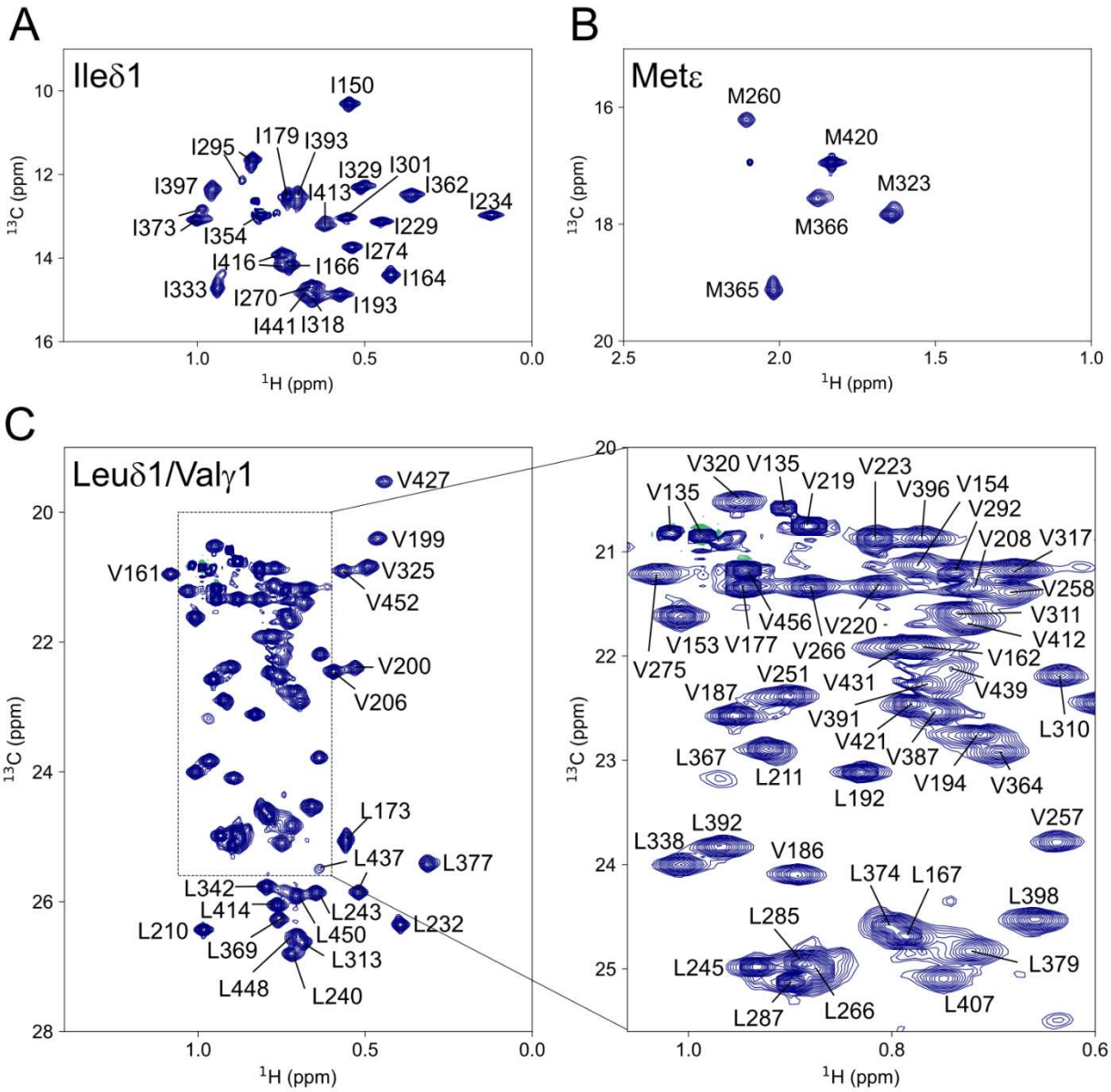

Fig. S1 Full assignment of Ileδ1, Metε, Leuδ1, and Valγ1 methyl groups. Selected regions of the ^{13}C-^{1}H HMQC spectrum of uniformly (U-)^{2}H, *proR* ILVM-labeled HtrA2 S306A (300 μM as a monomer), 23.5 Tesla (1 GHz ^{1}H frequency), 50 ºC, along with assignments of Ileδ1 (A), Metε (B) and Leuδ1/Valγ1 (C) methyls as shown.

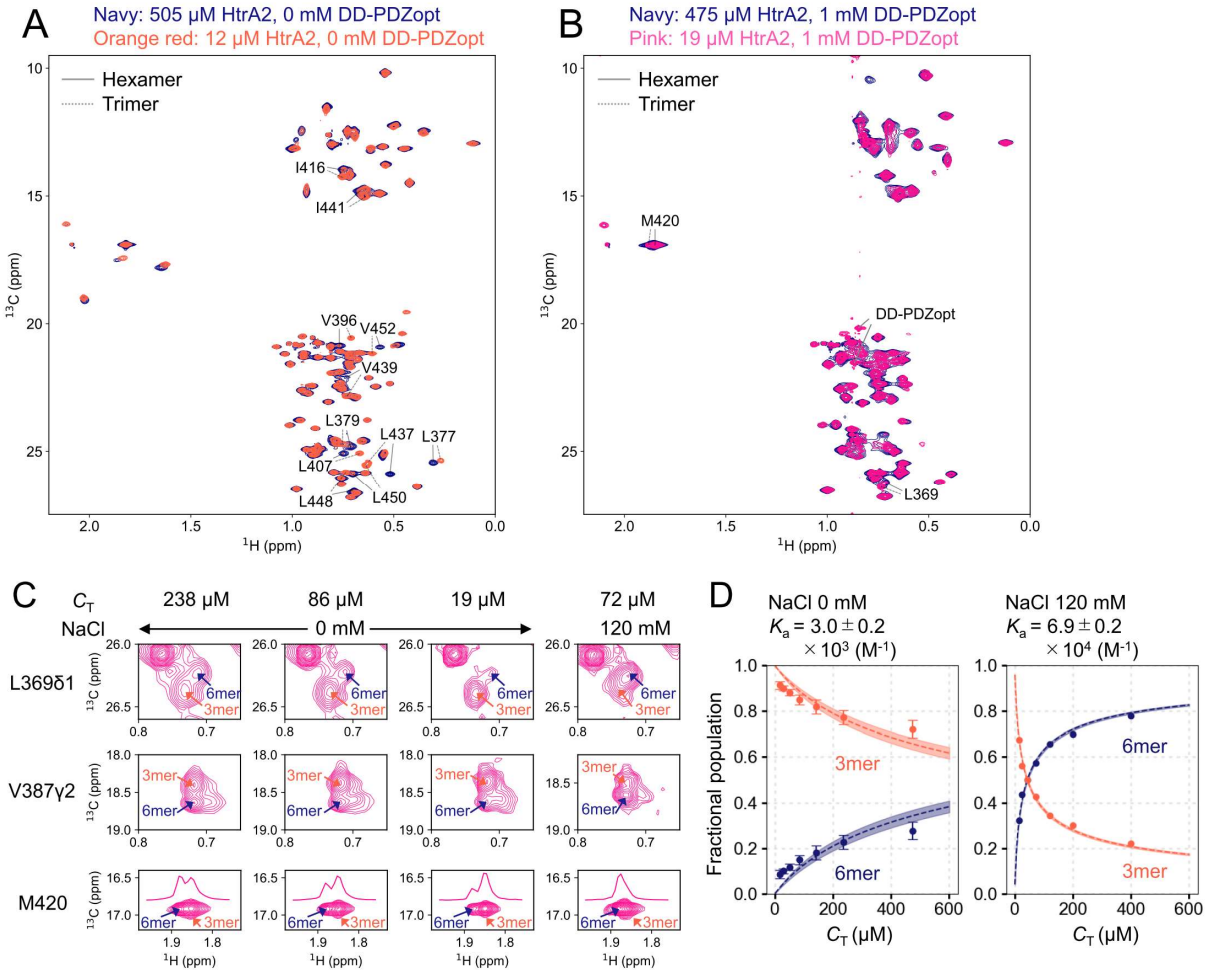

Fig. S2 ^{13}C-^{1}H HMQC spectra of HtrA2 with and without DD-PDZopt. ^{13}C-^{1}H HMQC spectra of U-^{2}H, *proR* ILVM HtrA2 S306A at high and low concentrations with (A) and without (B) 1 mM DD-PDZopt. The assignments of the methyl groups showing marked chemical shift differences are labeled. The identities of some of the hexamer (trimer) peaks are indicated by solid (dotted) lines, respectively. The C-terminal valine methyl signals from (natural abundance) DD-PDZopt are also highlighted. Hexamer and trimer populations were calculated to be 79% and 21 % at 505 μM and 24 % and 76 % at 12 μM in the free state using K_a of 5.2 × 10^4 M^{-1} (Fig. 2C); 28 % and 62 % at 475 μM, and 3 % and 97 % at 19 μM in the bound state using K_a of 3.0 × 10^3 M^{-1} (panel D). (C) Cross-peaks from selected methyl probes in ^{13}C-^{1}H HMQC spectra recorded with different protein concentrations in the presence of 1 mM DD-PDZopt used to quantify the trimer-hexamer equilibrium in the peptide bound state. A U-^{2}H, *proR* ILVM S306A HtrA2 sample was used to quantify peak intensities from L369δ1 and

M420, and a U-^{2}H, ILVM S306A HtrA2 sample was similarly used for V387γ2. ^{1}H 1D projections in the M420 spectra plot the maximum intensity in the displayed region. (D) Plots of fractional populations of hexameric (navy) and trimeric (orange-red) HtrA2 states calculated from L369δ1, V387γ2, and M420 methyl signal intensities as a function of protein concentration. Averaged values, based on calculated populations from the 3 methyl correlations, are shown with error-bars denoting 1 standard deviation (0 mM NaCl), while for the data at 120 mM NaCl the intensity values from V387γ2 only were used. The fitted trimer-hexamer association constants are indicated (dotted line is the best fitted curve and line thickness gives the 95% confidence interval of the fitted curve estimated from a Monte-Carlo error analysis). All spectra were recorded at 23.5 Tesla (1 GHz ^{1}H frequency), 40 ºC.

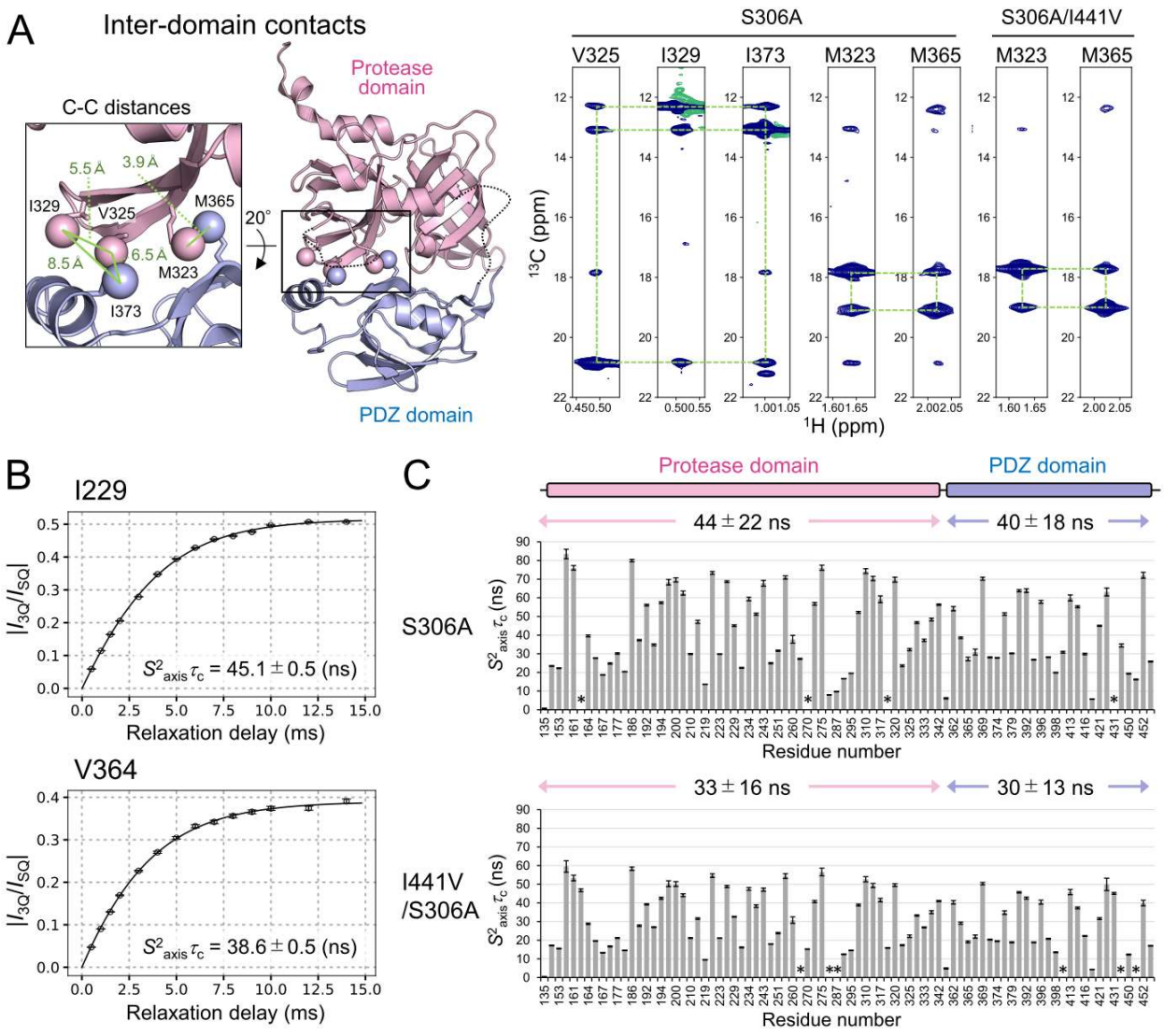

Fig. S3 HtrA2 inter-domain contacts are similar in the crystal and in solution. (A) Methyl groups showing strong inter-domain NOEs (PDB ID: 1LCY) (left) are consistent with expectations based on the X-ray structure. $^{13}C[F_1]$-$^{1}H[F_3]$ strips from a 3D $^{13}C[t_1]$-^{13}C $[t_2]$-^{1}H $[t_3]$ NOESY experiments (t_{mix} = 200 ms) highlighting selected methyl groups with inter-domain connectivities. Data recorded on samples of U-^{2}H, *proR* ILVM-labeled HtrA2 S306A (300 μM in monomer) and S306A/I441V (300 μM in monomer), 50 ºC, [NaCl] = 0 mM. (B) Representative plots of $|I_{3Q}/I_{SQ}|$ as a function of relaxation delay recorded using a U-^{2}H, *proR* ILVM-labeled HtrA2 S306A sample (300 μM in monomer), at 50 ºC. Profiles of I229 from the protease domain and V364 from the PDZ domain are

shown. (C) Plots of the product of the order parameter squared of the methyl group symmetry axis and the overall rotational correlation time ($S^2_{axis}\tau_c$) as a function of residue for U-^{2}H, *proR* ILVM-labeled HtrA2 S036A (300 μM monomer) (top) and U-^{2}H, *proR* ILVM-labeled HtrA2 I441V/S306A (300 μM in monomer) (bottom), 50 °C. Average $S^2_{axis}\tau_c$ values (average ± one standard deviation) for the protease and PDZ domains are displayed on the top of the plot. Asterisks indicate methyl groups that could not be analyzed due to peak overlaps.

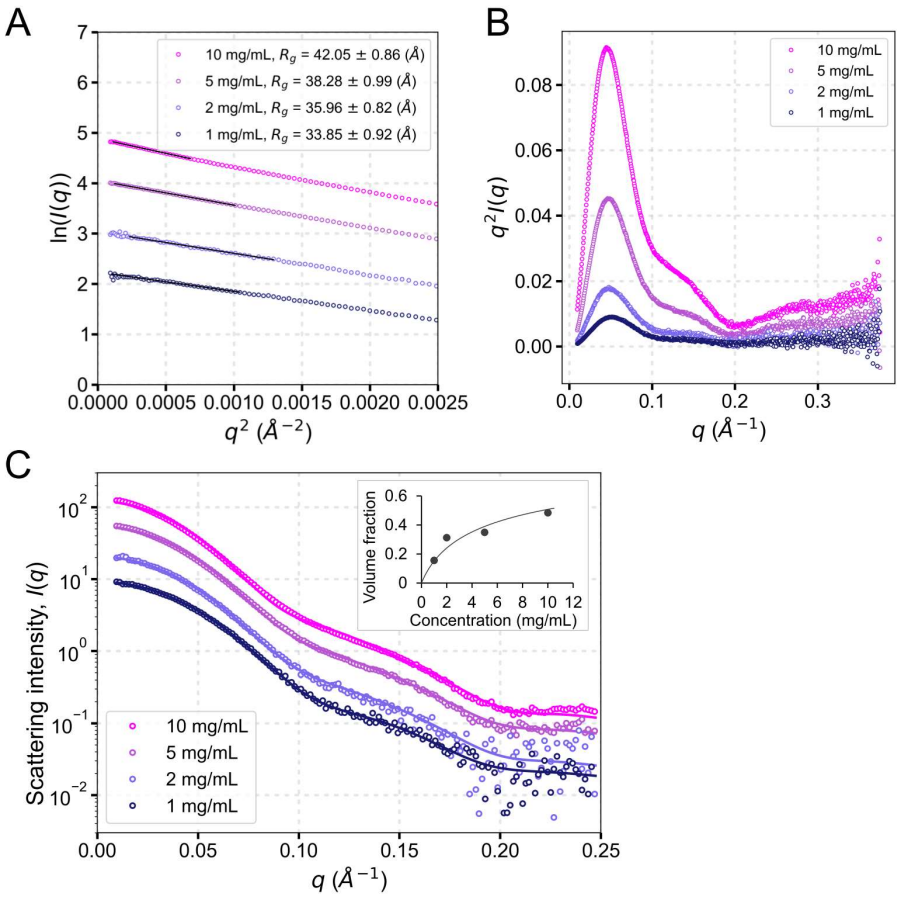

Fig. S4 SAXS profiles of HtrA2. (A) Guinier plots of S306A HtrA2 SAXS profiles at 4 different protein concentrations (circles). The fitted Guinier curves in the low q range are shown as black lines, establishing that there is no significant aggregation or particle interference. Calculated R_g values are listed in the inset. (B) Kratky plots of S306A HtrA2 SAXS profiles at 4 different protein concentrations (circles) establish that the particles are globular. (C) SAXS profiles of S306A HtrA2 at

4 different protein concentrations (circles). Solid lines are fitted curves back-calculated from the trimer-hexamer structural ensemble. The plot of the fitted volume fraction of the hexamer as a function of protein concentration is shown as in inset (hexamer volume fractions of 0.16, 0.31, 0.35, and 0.48 for protein concentrations of 1, 2, 5, and 10 mg/mL). All SAXS profiles were measured at 23-26 ºC in high salt buffer (120 mM NaCl).

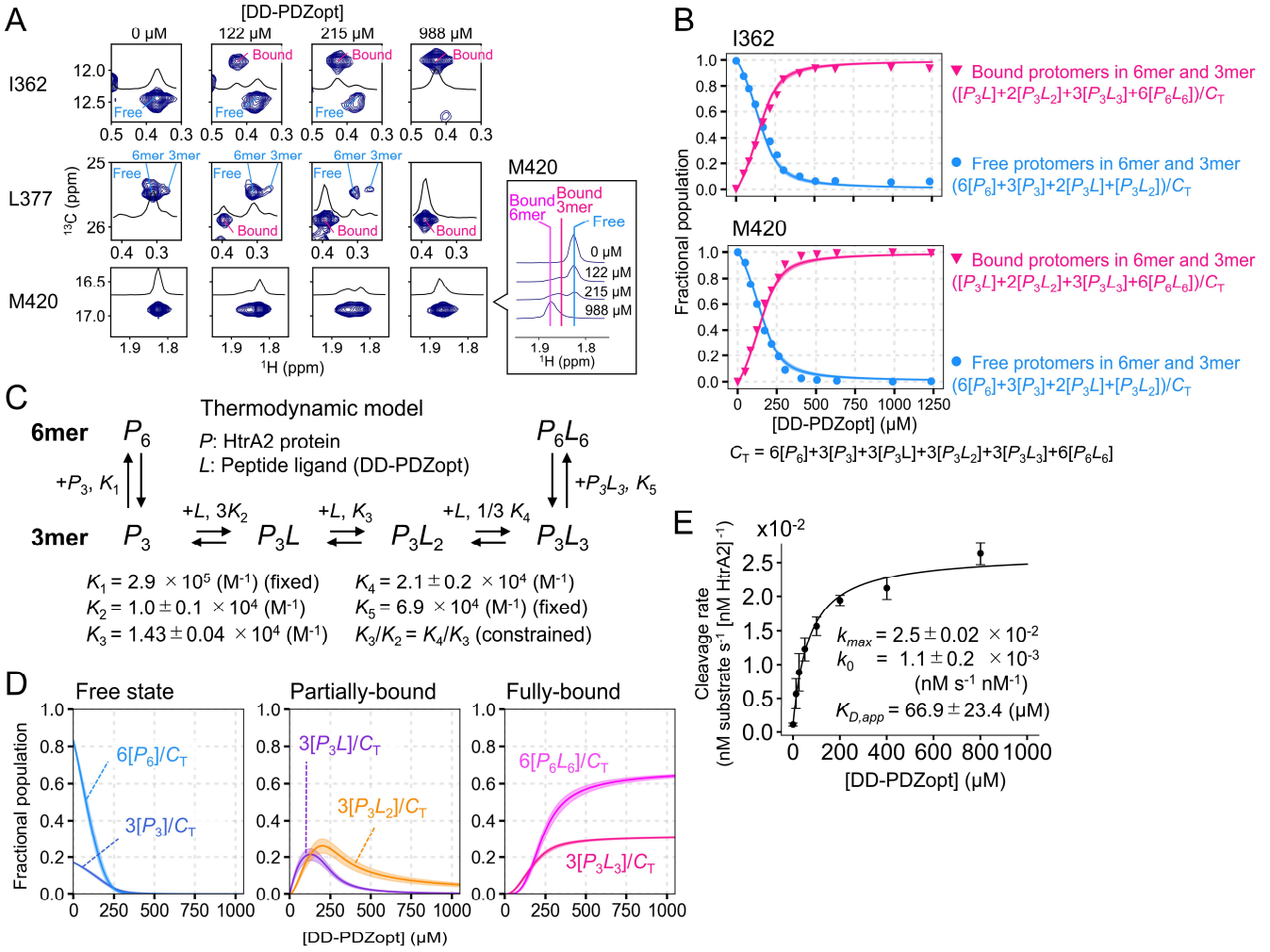

Fig. S5 DD-PDZopt titration at [NaCl] = 120 mM. (A) Spectral changes for I362, L377, and M420 of U-^{2}H, *proR* ILVM-labeled HtrA2 S306A (150 μM in monomer) as a function of DD-PDZopt concentration, 40 ºC. ^{1}H 1D projections show maximum intensities in the displayed ^{13}C region. The oligomerization and the peptide-binding states of each signal are noted. (B) Plots of fractional

populations of states, as indicated, calculated from the signal intensities of I362 and M420. Expressions for the populations are indicated, where C_T denotes the total protein concentration. Dotted lines are the fitted curves, with the line thickness representing the 95% confidence interval of the fitted curve as estimated from a Monte-Carlo error analysis. (C) Thermodynamics of DD-PDZopt binding to HtrA2, 120 mM NaCl, 40 °C. K_1 and K_5 values were fixed to those obtained from the dilution experiments (Figs. 2C & *SI Appendix* Fig. S2D), and K_2, K_3, and K_4 values were constrained such that $K_3/K_2 = K_4/K_3$. The fitted values obtained are listed (See *SI Appendix*, "II) Fits of thermodynamics (*c*) *Model 3: step-wise ligand binding to trimer with cooperativity*" for further details. (D) Fractional populations of protomers in each state as a function of [DD-PDZopt] calculated using fitted equilibrium constants (dark line, with the line thickness corresponding to the 95% confidence interval estimated from a Monte-Carlo error analyses). (E) Plot of cleavage rate of fluorescent substrate peptide as a function of [DD-PDZopt] measured in the presence of 120 mM NaCl, 40 °C. Data points are the average ± one standard deviation based on three repeat measurements, fit to a standard one-site binding model (solid line).

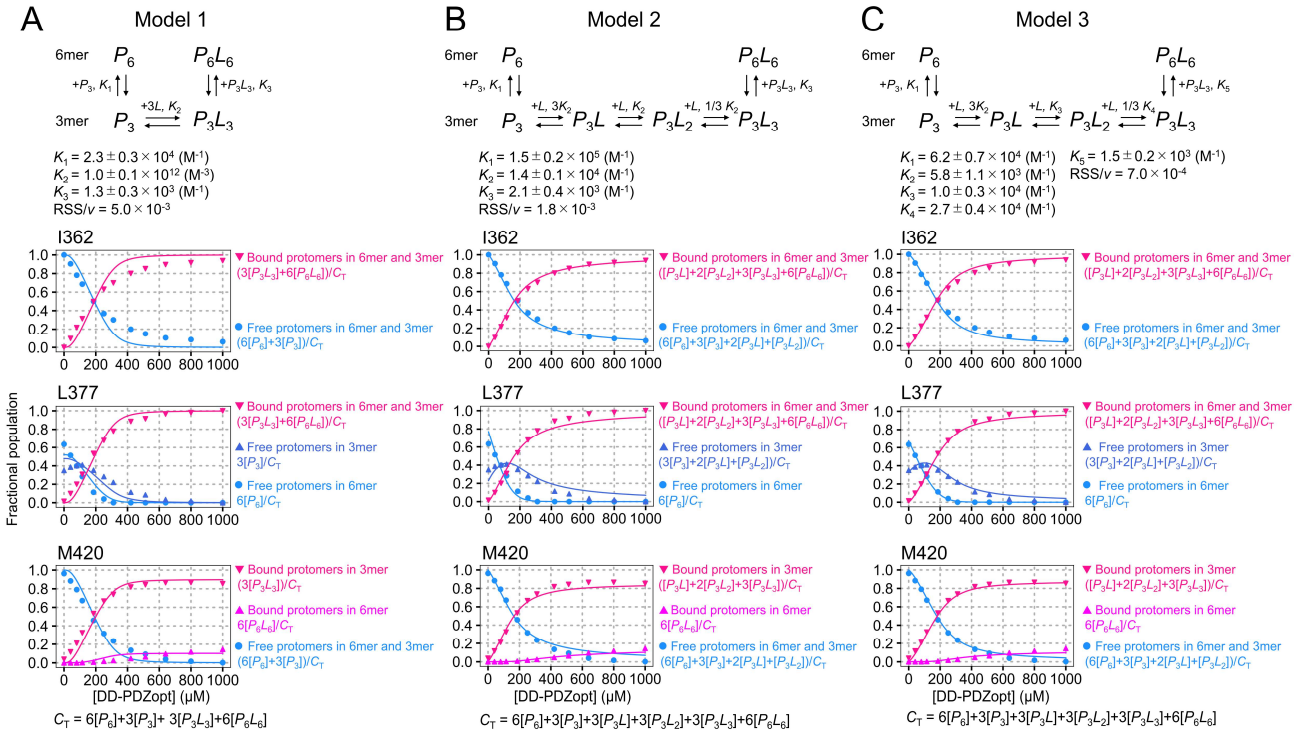

Fig. S6 Different thermodynamic models used to fit DD-PDZopt titration profiles. (A) Model 1 in which all three DD-PDZopt molecules simultaneously bind to an HtrA2 trimer. (B) Model 2 assumes a

step-wise binding of DD-PDZopt to the HtrA2 trimer with the same microscopic binding affinities in each step. (C) Model 3, as Model 2 but where the binding of DD-PDZopt to the HtrA2 trimer occurs with the different affinities. This model is the same as that shown in Fig. 5C. The fitted binding profiles (solid lines) for I366, L377, and M420 are shown for each model, along with the fitted parameters below each of the schemes and RSS/v values (see text). Errors were estimated from Monte-Carlo error analyses.

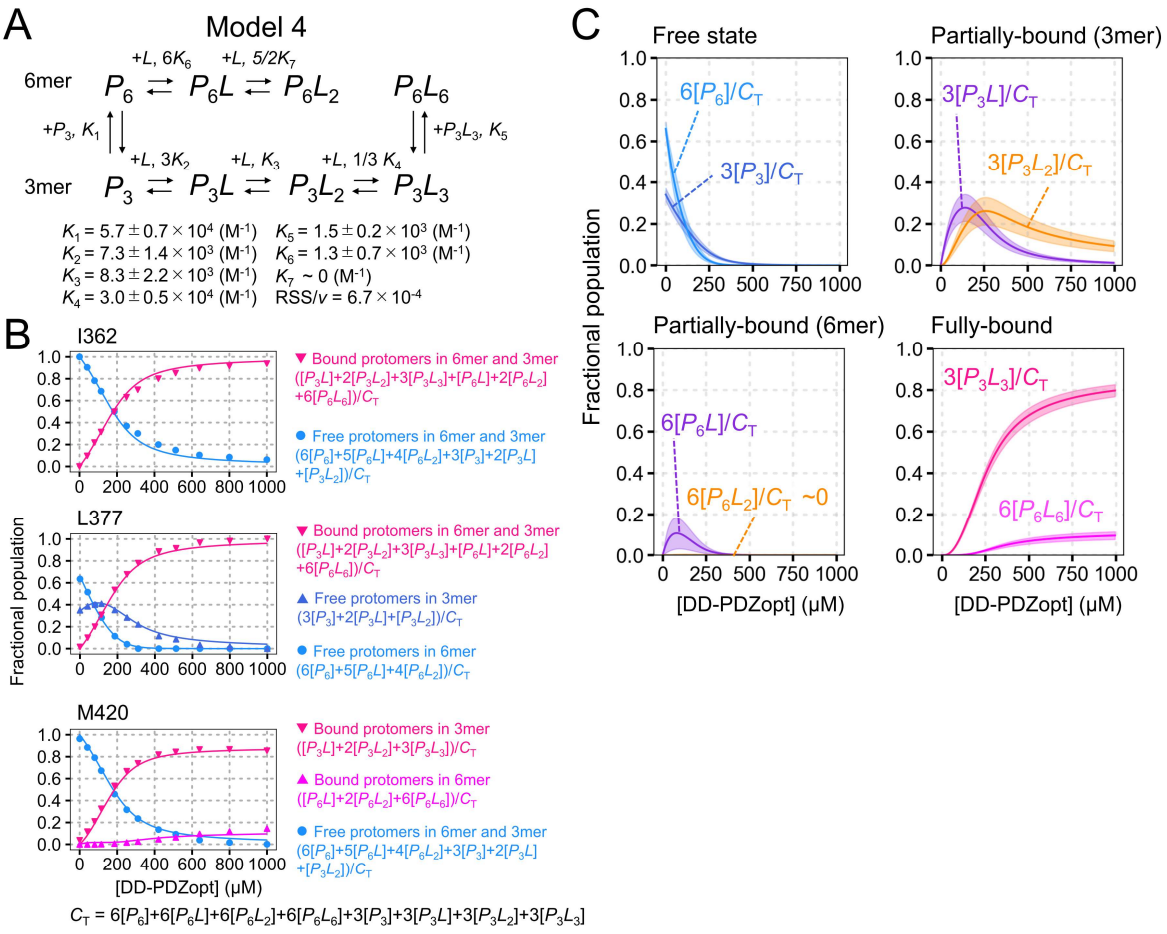

Fig. S7 Thermodynamic model including partial binding to the hexamer state. (A) Schematic of model 4 along with fitted results based on a combined analysis of profiles from I362, L377, and M420 (B). (B) and (C) Details as in Fig. 5 and *SI Appendix* S5.

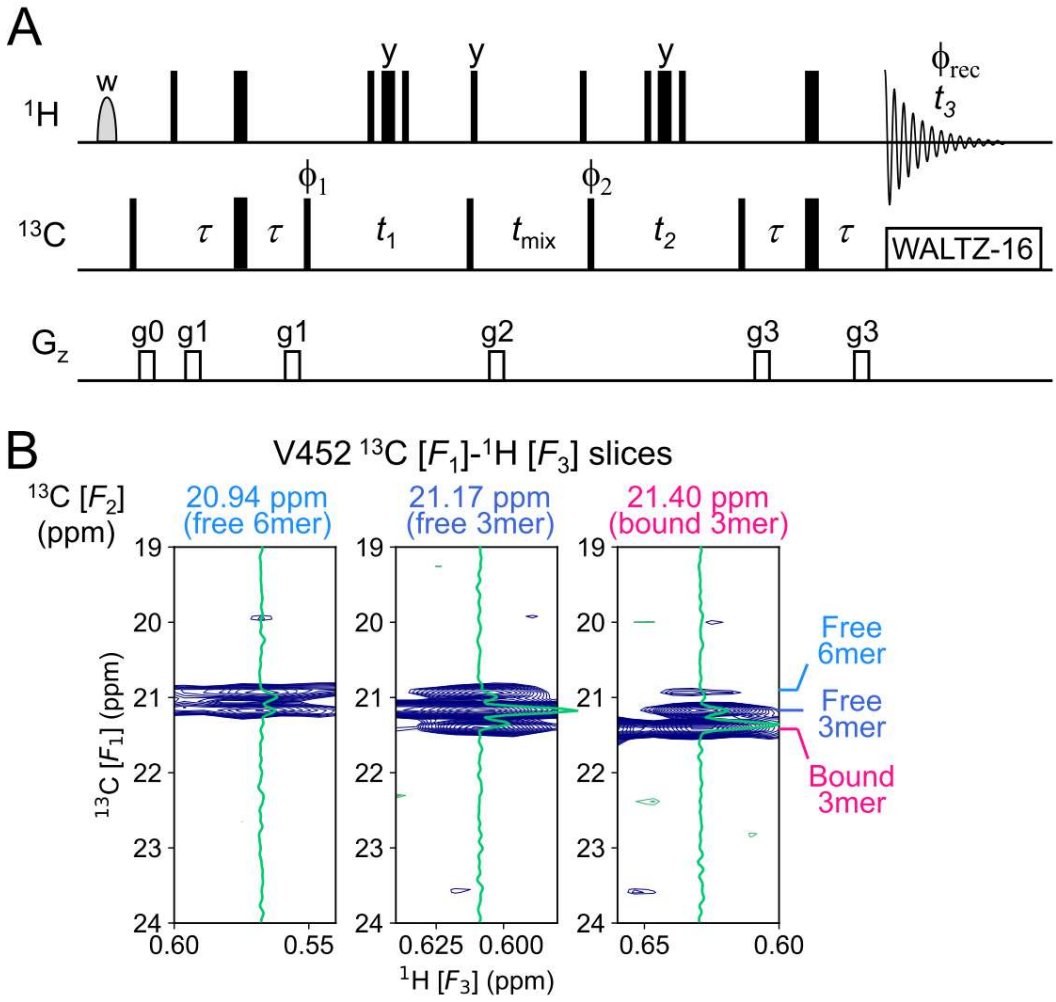

Fig. S8 Pulse sequence for the 3D ZZ-exchange experiment and data from V452 (A) Pulse scheme for the 3D ^{13}C[t_1]-t_{mix}-^{13}C[t_2]-^{1}H[t_3] ZZ-exchange experiment. 90° (180°) rectangular pulses, denoted by narrow (wide) bars, are applied at maximum power. All pulses are applied along the *x*-axis unless otherwise indicated The water-selective shaped pulse marked with "w" (~7 ms) is implemented using the EBURP-1 profile (24) centered on the water resonance (~4.7 ppm); the ^{1}H carrier is subsequently moved to the methyl region (~1.0 ppm) for the remainder of the scheme. The ^{13}C carrier is set to 19 ppm. The ^{13}C WALTZ-16 decoupling element (25) is applied with field of 2.25 kHz. The delay τ is set to 1.8 ms (=1/4J_{CH}) The phase cycle is $\varphi1 = x, -x$; $\varphi2 = 2x, 2(-x)$; $\varphi_{rec} = x, -x, -x, x$. Quadrature detection in F_1 and F_2 is achieved by STATES-TPPI (26) of φ1 and φ2, respectively. Gradients are applied with the following durations (ms) and strengths (in % maximum): g0: (1.0, 25%), g1: (0.5, 30%), g2: (1.0, 50%),

g3: (0.6, 30%). (B) ^{13}C [F_1]-^{1}H [F_3] slices from the 3D ZZ-exchange experiment, mixing time = 50 ms, focusing on V452. Regions with distinct ^{13}C[F_2] chemical shifts for V452 (20.94 ppm for the free hexamer, 21.17 ppm for the free trimer, and 21.4 ppm for the bound trimer) are shown. ^{13}C[F_1] 1D slices at the center of the peak are indicated by green lines in each strip. The sample is comprised of 160 μM (monomer) U-^{2}H, *proR* ILVM S306A HtrA2 and 100 μM U-^{2}H labeled DD-PDZopt, 0 mM NaCl, 40 °C.

SI References

1. V. Tugarinov, V. Kanelis, L. E. Kay, Isotope labeling strategies for the study of high-molecular-weight proteins by solution NMR spectroscopy. *Nat. Protoc.* **1**, 749–754 (2006).

2. P. Gans, *et al.*, Stereospecific Isotopic Labeling of Methyl Groups for NMR Spectroscopic Studies of High-Molecular-Weight Proteins. *Angew. Chem. Int. Ed.* **49**, 1958–1962 (2010).

3. V. Tugarinov, P. M. Hwang, J. E. Ollerenshaw, L. E. Kay, Cross-correlated relaxation enhanced ^{1}H-^{13}C NMR spectroscopy of methyl groups in very high molecular weight proteins and protein complexes. *J. Am. Chem. Soc.* **125**, 10420–8 (2003).

4. L. E. Kay, Artifacts can emerge in spectra recorded with even the simplest of pulse schemes: an HMQC case study. *J. Biomol. NMR* **73**, 423–427 (2019).

5. F. Delaglio, *et al.*, NMRPipe: A multidimensional spectral processing system based on UNIX pipes. *J. Biomol. NMR* **6**, 277–293 (1995).

6. J. J. Helmus, C. P. Jaroniec, Nmrglue: an open source Python package for the analysis of multidimensional NMR data. *J. Biomol. NMR* **55**, 355–367 (2013).

7. S. G. Hyberts, K. Takeuchi, G. Wagner, Poisson-gap sampling and forward maximum entropy reconstruction for enhancing the resolution and sensitivity of protein NMR data. *J. Am. Chem.*

Soc. **132**, 2145–2147 (2010).

8. J. Ying, F. Delaglio, D. A. Torchia, A. Bax, Sparse multidimensional iterative lineshape-enhanced (SMILE) reconstruction of both non-uniformly sampled and conventional NMR data. *J. Biomol. NMR* **68**, 101–118 (2017).

9. H. Sun, L. E. Kay, V. Tugarinov, An optimized relaxation-based coherence transfer NMR experiment for the measurement of side-chain order in methyl-protonated, highly deuterated proteins. *J. Phys. Chem. B* **115**, 14878–14884 (2011).

10. W. Li, *et al.*, Structural insights into the pro-apoptotic function of mitochondrial serine protease htra2/omi. *Nat. Struct. Biol.* **9**, 436–441 (2002).

11. M. P. Latham, A. Sekhar, L. E. Kay, Understanding the mechanism of proteasome 20S core particle gating. *Proc. Natl. Acad. Sci. USA* **111**, 5532–5537 (2014).

12. R. W. Harkness, Y. Toyama, L. E. Kay, Analyzing multi-step ligand binding reactions for oligomeric proteins by NMR: Theoretical and computational considerations. *J. Magn. Reson.* **318**, 106802 (2020).

13. A. G. Palmer, C. D. Kroenke, J. P. Loria, NMR methods for quantifying microsecond-to-millisecond motions in biological macromolecules. *Methods Enzym.* **339**, 204–238 (2001).

14. A. Sekhar, A. D. Bain, J. A. O. Rumfeldt, E. M. Meiering, L. E. Kay, Evolution of magnetization due to asymmetric dimerization: Theoretical considerations and application to aberrant oligomers formed by apoSOD1^{2SH}. *Phys. Chem. Chem. Phys.* **18**, 5720–5728 (2016).

15. E. Rennella, A. Sekhar, L. E. Kay, Self-Assembly of Human Profilin-1 Detected by Carr–Purcell–Meiboom–Gill Nuclear Magnetic Resonance (CPMG NMR) Spectroscopy. *Biochemistry* **56**, 692–703 (2017).

16. W. H. Press, B. P. Flannery, S. A. Teukolsky, W. T. Vetterling, Numerical Recipes in C. The Art of Scientific Computing 2nd edn (Cambridge Univ. Press, 1992).

17. M. V. Petoukhov, *et al.*, New developments in the ATSAS program package for small-angle scattering data analysis. *J. Appl. Crystallogr.* **45**, 342–350 (2012).

18. N. R. Hajizadeh, D. Franke, C. M. Jeffries, D. I. Svergun, Consensus Bayesian assessment of protein molecular mass from solution X-ray scattering data. *Sci. Rep.* **8**, 7204 (2018).

19. P. V. Konarev, V. V. Volkov, A. V. Sokolova, M. H. J. Koch, D. I. Svergun, PRIMUS: A Windows PC-based system for small-angle scattering data analysis. *J. Appl. Crystallogr.* **36**, 1277–1282 (2003).

20. S. Classen, *et al.*, Implementation and performance of SIBYLS: A dual endstation small-angle X-ray scattering and macromolecular crystallography beamline at the Advanced Light Source. *J. Appl. Crystallogr.* **46**, 1–13 (2013).

21. M. V. Petoukhov, D. I. Svergun, Global rigid body modeling of macromolecular complexes against small-angle scattering data. *Biophys. J.* **89**, 1237–1250 (2005).

22. A. Waterhouse, *et al.*, SWISS-MODEL: homology modelling of protein structures and complexes. *Nucleic Acids Res.* **46**, W296–W303 (2018).

23. L. M. Martins, *et al.*, Binding specificity and regulation of the serine protease and PDZ domains

of HtrA2/Omi. *J. Biol. Chem.* **278**, 49417–49427 (2003).

24. H. Geen, R. Freeman, Band-selective radiofrequency pulses. *J. Magn. Reson.* **93**, 93–141 (1991).

25. A. J. Shaka, J. Keeler, T. Frenkiel, R. Freeman, An improved sequence for broadband decoupling: WALTZ-16. *J. Magn. Reson.* **52**, 335–338 (1983).

26. D. Marion, M. Ikura, R. Tschudin, A. Bax, Rapid recording of 2D NMR spectra without phase cycling. Application to the study of hydrogen exchange in proteins. *J. Magn. Reson.* **85**, 393–399 (1989).